

RRL Solar

Rapid Research Letters
Full Papers · Reviews

Perovskite Solar Cells

In article number 2000093, Ming-Chung Wu, Kun-Mu Lee, and co-workers use polyethylene glycol (PEG) as an additive for the perovskite active layer in lead-reduced perovskite solar cells. The PEG can effectively control the surface morphology of the perovskite film and improve the charge carrier transport. For 10% lead-reduced perovskite solar cells, a champion power conversion efficiency of 16.1% is obtained without significant hysteresis.

Polymer Additives for Morphology Control in High-Performance Lead-Reduced Perovskite Solar Cells

Ming-Chung Wu,* Yi-Ying Li, Shun-Hsiang Chan, Kun-Mu Lee,* and Wei-Fang Su

The organic–inorganic halide perovskite solar cells (PSCs) are rapidly developed in just a few years due to its high power conversion efficiency. However, it still faces some critical issues, one of which is the presence of toxic lead (Pb^{2+}). Recent researches show that barium (Ba^{2+}) can partially replace the Pb^{2+} in perovskite structure and achieve a promising device performance because of its adequate ionic radius. However, the optimal replacement amount of Ba^{2+} in perovskite is still limited. Herein, the methylammonium (MA)/formamidinium (FA) mixed-cation perovskite is used as the active layer in PSCs and Pb^{2+} is partially substituted with Ba^{2+} . Compared with the pure MA system, the best device efficiency can be achieved using higher Ba^{2+} replacement ratio. In addition, while introducing the appropriate polymer additive, the replacement ratio can be further increased without compromise of device efficiency. Using polyethylene glycol as polymer additive, 10.0 mol% Ba-doped MA/FA mixed-cation PSC with an efficiency of 16.1% can be realized. It is believed that this report provides an effective strategy to fabricate high-performance lead-reduced PSCs.

addressed, such as hysteresis effect,^[8] instability of PSCs,^[9] and the toxicity of lead (Pb).^[10] Typically, the hysteresis effect results from the current difference in the reverse and forward scan, which results in an inaccurate estimate of the device's PCE.^[11] It is speculated that the origin of the hysteresis effect is due to the charge carriers, conductivity modification, ferroelectricity, and ion migration.^[12,13] The typical perovskite structure, $\text{CH}_3\text{NH}_3\text{PbI}_3$ (MAPbI₃), usually suffers from moisture, heat, and irradiation, which will lead to the induced trap-state formation and halide segregation.^[14,15] The toxicity of lead is the most crucial problem to be solved. When lead builds up in our bodies, it causes serious health problems, such as headaches, irritability, reduced sensations, aggressive behavior, difficulty sleeping, and so on.^[16] Moreover, lead is even more harmful to children as it affects nerves

1. Introduction

Organic–inorganic halide perovskite solar cells (PSCs) have been rapidly developed and have reached to a high power conversion efficiency (PCE) of 25.2% recently.^[1] There are many advantages of PSCs, including tunable bandgap, low cost, solution process, flexibility, excellent light absorption, fast charge-carrier mobility, and so on.^[2–7] However, there are still some issues to be

and brain development. If the Pb content in perovskite can be replaced, it would be much friendlier to the environment and would possess the great potential for PSCs to be commercialized.


Because long-term exposure to Pb is harmful to the human body, lead-reduced and lead-free perovskite materials have been developed in recent years.^[17] Alkaline earth metals, such as magnesium (Mg),^[18] calcium (Ca),^[19] strontium (Sr),^[20,21] and barium (Ba),^[22] are able to retain lattice structure, and thus can replace lead according to Goldschmidt's rules.^[20,23] In addition, alkaline earth metals can remain balanced charge. They are also stable and abundant on earth.^[24] MACaI_3 , MASrI_3 , and MABaI_3 alkaline earth metal perovskites have been suggested to improve the stability of perovskite structure. Also, according to the previous work done by our research group, Ba^{2+} is the most suitable for Pb^{2+} replacement with better photovoltaic properties and improved stability.^[22] The incorporation of Ba^{2+} in perovskite stabilizes the black phase of CsPbX_3 , approaching high-stability all-inorganic lead-halide perovskites.^[25] From a previous study, we suggested that the doping of Ba^{2+} leads to higher perovskite structure thermal stability as Ba has a higher melting point than Pb.^[26] Moreover, it was reported that with Ba^{2+} doping the crystallinity and surface morphology can be improved, and the trap density, electron–hole recombination, and hysteresis effect were significantly reduced.^[27] All of these properties contributed to excellent device performance. Barium cation was also utilized to stabilize the perovskite structure by interface modification. By the ultrathin BaTiO_3 layer modification on the mesoporous TiO_2 layer, the charge recombination was suppressed and

Dr. M.-C. Wu, Y.-Y. Li, Dr. S.-H. Chan, Dr. K.-M. Lee
Department of Chemical and Materials Engineering
Chang Gung University
Taoyuan 33302, Taiwan
E-mail: mingchungwu@cgu.edu.tw; kmlee@mail.cgu.edu.tw

Dr. M.-C. Wu, Dr. S.-H. Chan, Dr. K.-M. Lee
Green Technology Research Center
Chang Gung University
Taoyuan 33302, Taiwan

Dr. M.-C. Wu, Dr. K.-M. Lee
Division of Neonatology
Department of Pediatrics
Chang Gung Memorial Hospital
Linkou, Taoyuan 33305, Taiwan

Dr. W.-F. Su
Department of Materials Science and Engineering
National Taiwan University
Taipei 10617, Taiwan

 The ORCID identification number(s) for the author(s) of this article can be found under <https://doi.org/10.1002/solr.202000093>.

DOI: 10.1002/solr.202000093

the electron extraction rate at the interface was enhanced effectively, leading to better photovoltaic performance of PSCs.^[28]

Adding polymer additive into the perovskite layer has become a promising method to improve the perovskite device performance, which may result in better morphology, crystallinity, and improve the coverage between perovskite layers.^[29] Moreover, it has been reported that the more compact perovskite film can be formed with the addition of long-chain polymers in a previous study.^[30] Polyvinyl butyral (PVB) and polyvinyl alcohol (PVA) can both improve the perovskite film as polymer additives. For example, the perovskite film with PVB has higher crystallinity and smoother surface, which improves the film quality and results in better device performance and stability.^[31] With the addition of polymeric Lewis base into perovskite, a long-range molecularly ordered intermediate phase forms to increase the activation energy of nucleation and the precursor molecules diffusion, which results in higher crystallinity and larger grains.^[32] In a previous study, two novel polymeric semiconductors with large perfluorinated chains are performed as polymer additives in PSCs. The perfluorinated compound forms a protective barrier that can protect the perovskite layer from oxygen and humidity and improve device stability.^[33] Polyethylene glycol (PEG) as a polymer additive improves the humidity resistant of perovskite with self-healing behavior.^[34]

In this work, we introduce an optimized-ratio reduced-lead mixed-cation perovskite material. There are many advantages

to using mixed-cation perovskite as absorber, such as lower bandgap, wider absorption range, excellent electronic properties, and high PCE.^[35] In contrast, alkaline-earth metal cations are the prior choice for Pb replacement according to previous studies. Among alkaline-earth metal cations, barium cation (Ba^{2+}) was chosen as our replacement candidate, due to its great performance which was shown in the previous studies and the research done by our research group. While incorporating formamidinium (FA) into perovskite and using MA/FA mixed-cation perovskite as our control, according to Goldschmidt equation, it is proposed that the replacement ratio of Ba^{2+} can be increased due to larger ionic radius of Ba^{2+} over Pb^{2+} . Nevertheless, excessive replacement of Pb^{2+} by Ba^{2+} may result in unstable perovskite structure and lead to inferior photovoltaic properties and poor morphology. To solve this problem, polymer additives, including poly(vinylidene fluoride-co-trifluoroethylene) [P(VDF-TrFE)],^[36,37] polymethyl methacrylate (PMMA),^[38–40] and PEG,^[41–43] were added into the lead-reduced mixed-cation perovskite to modify the perovskite films.

P(VDF-TrFE) was chosen as one of the useful polymer additives mainly because of its excellent UV resistance,^[44] which is expected to improve device stability. P(VDF-TrFE) is also a ferroelectric copolymer with excellent clarity. PMMA is a polymer

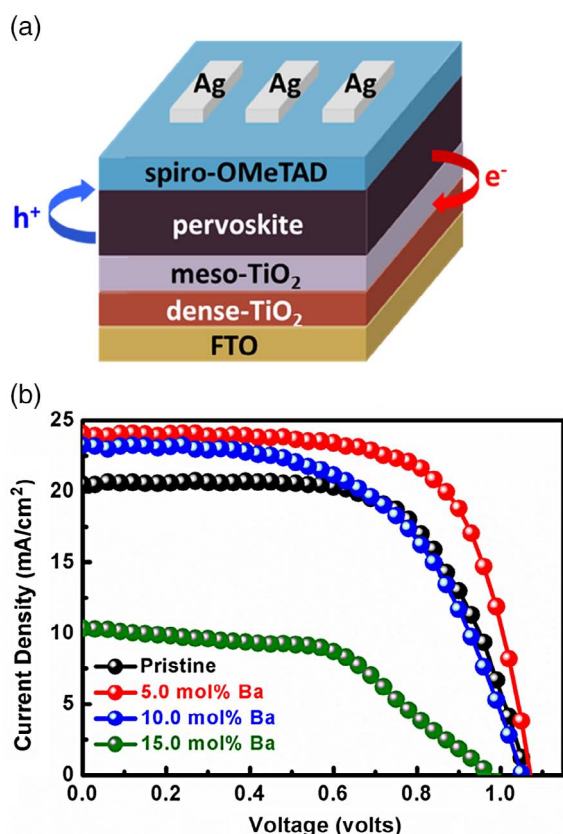


Figure 1. a) Schematic diagram of the high-performance lead-reduced PSC. b) J–V curves of PSCs devices with 5.0, 10.0, and 15.0 mol% Ba doping.

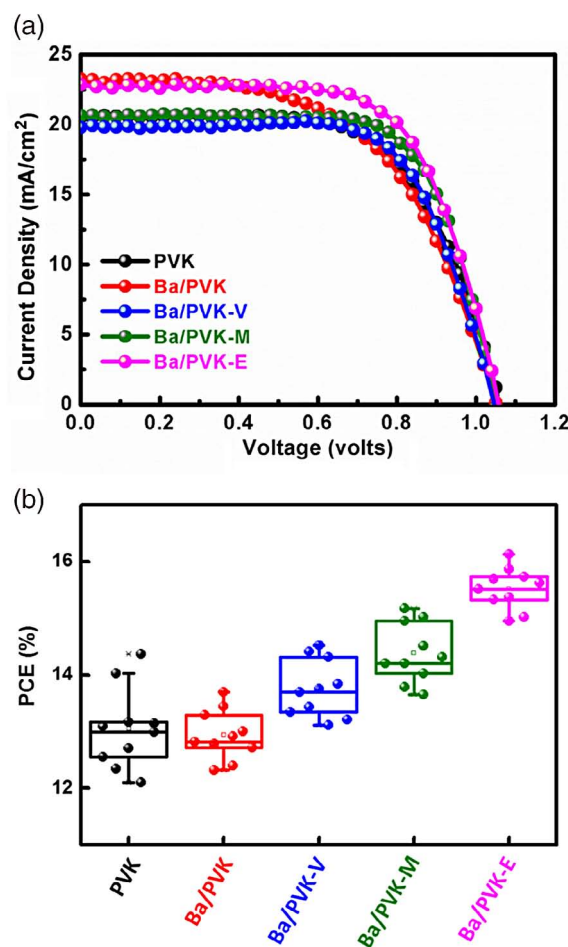


Figure 2. a) J–V curves and b) PCE distributions with ten devices of PVK, Ba/PVK, Ba/PVK-V, Ba/PVK-M, and Ba/PVK-E.

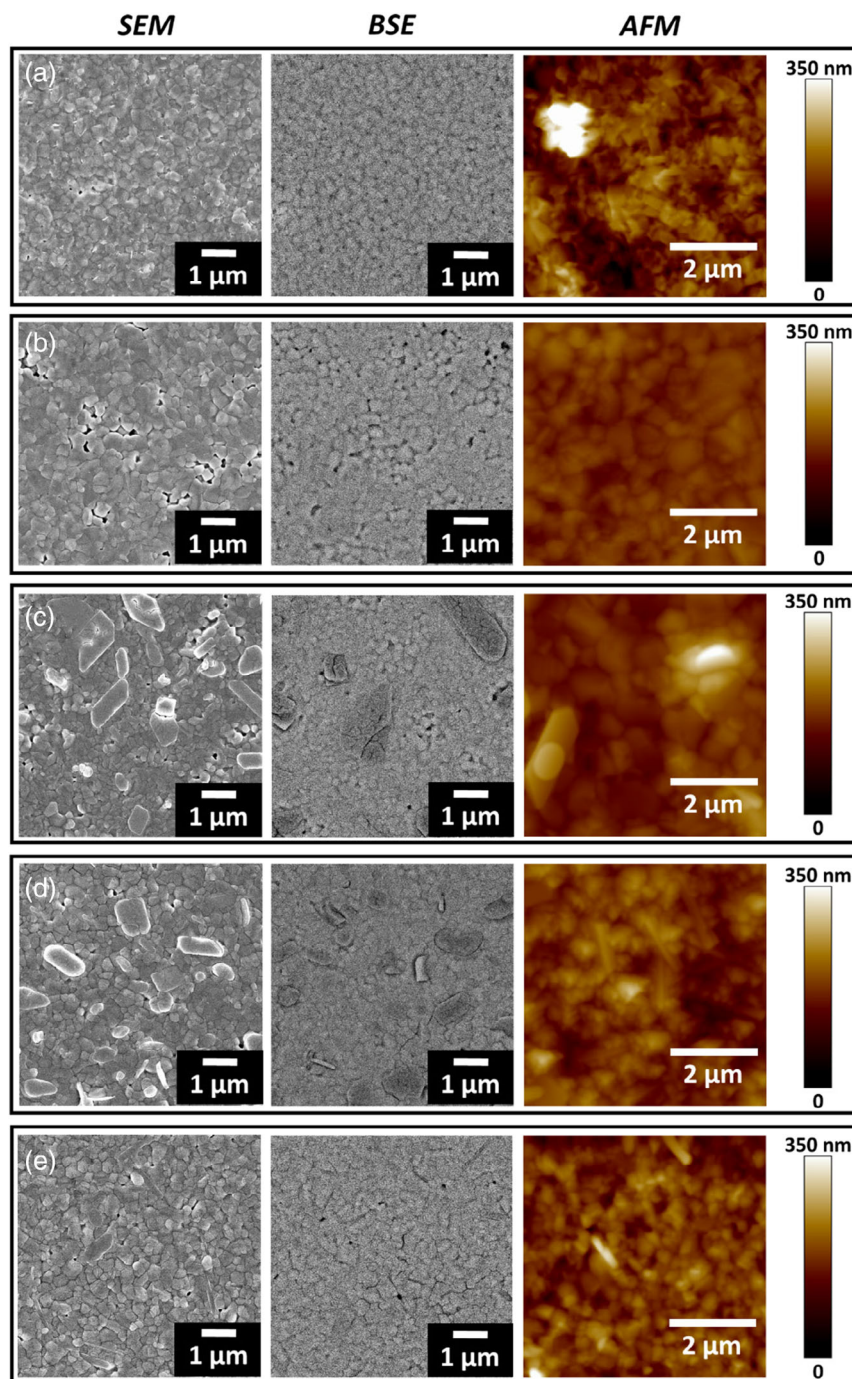


Figure 3. FE-SEM (left column), BSE (middle column), and AFM images (right column) of a) PVK, b) Ba/PVK, c) Ba/PVK-V, d) Ba/PVK-M, and e) Ba/PVK-E perovskite films.

that is extensively used in optical applications.^[45,46] Outstanding characteristics of transparency (up to 92% of the light passing through),^[47] weatherability,^[48] and scratch resistance^[49] make PMMA one of the more reliable polymer additive candidates. PEG is beneficial for solubility of water and other solvents. PEG has low volatility which translates to high thermal stability for various applications. For such valuable properties, PEG is certainly

considered as a polymer additive to apply to our mixed-cation lead-reduced PSCs. Concluding the advantages of these polymers mentioned previously, P(VDF-TrFE), PMMA, and PEG were chosen as our polymer additives to be doped into the mixed-cation lead-reduced perovskite device, hoping to improve the morphology and photovoltaic properties. The polymers are added into the perovskite precursor solution with various concentrations

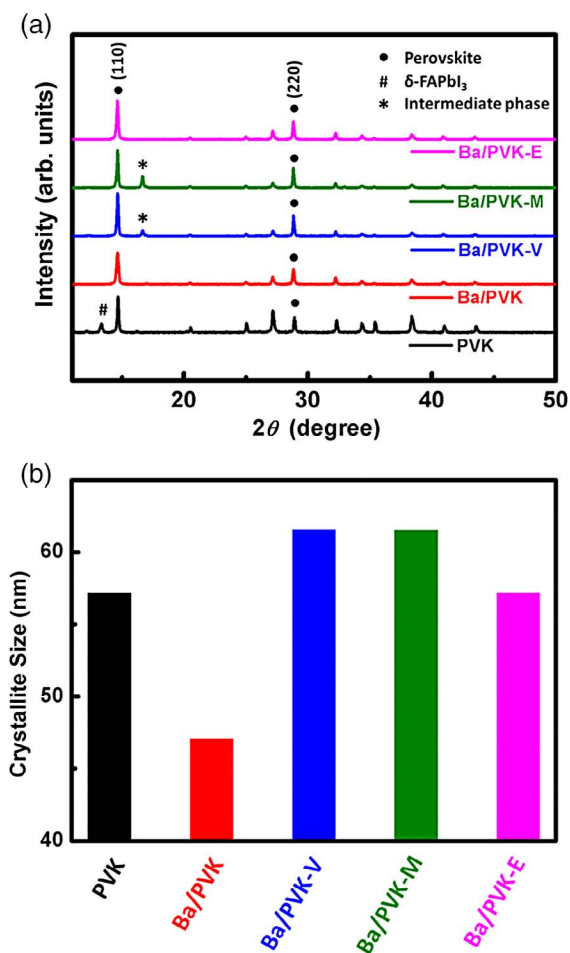


Figure 4. a) XRD pattern and b) crystallite size of PVK, Ba/PVK, Ba/PVK-V, Ba/PVK-M, and Ba/PVK-E perovskite films.

to compare the perovskite material properties. The relationship between polymer additives and perovskite phase will be discussed in-depth, and further analysis made on perovskite materials will be investigated.

2. Results and Discussion

The Ba-doped PSCs with various concentrations (5.0, 10.0, and 15.0 mol%) were fabricated to determine the photovoltaic performance of the lead-reduced devices comparing with the pristine mixed-cation PSCs without Ba doping (abbreviated as PVK). The schematic diagram of the PSCs fabricated in this study is shown in Figure 1a. Figure 1b shows the *J*–*V* curves of Ba-doped devices with various doping concentrations. At 5.0 mol% of Ba doping, the device exhibited the best performance, achieving PCE of 17.52% with high *V*_{oc} of 1.07 V, *J*_{sc} of 24.06 mA cm^{−2}, and FF of 67.98%. According to our previous work, doping barium into perovskite has several advantages, such as improving surface morphology, increasing crystallinity, and facilitating charge carrier transport.^[22] However, when the amount of Ba doping was further increased to 10.0 mol% or even to 15.0 mol%,

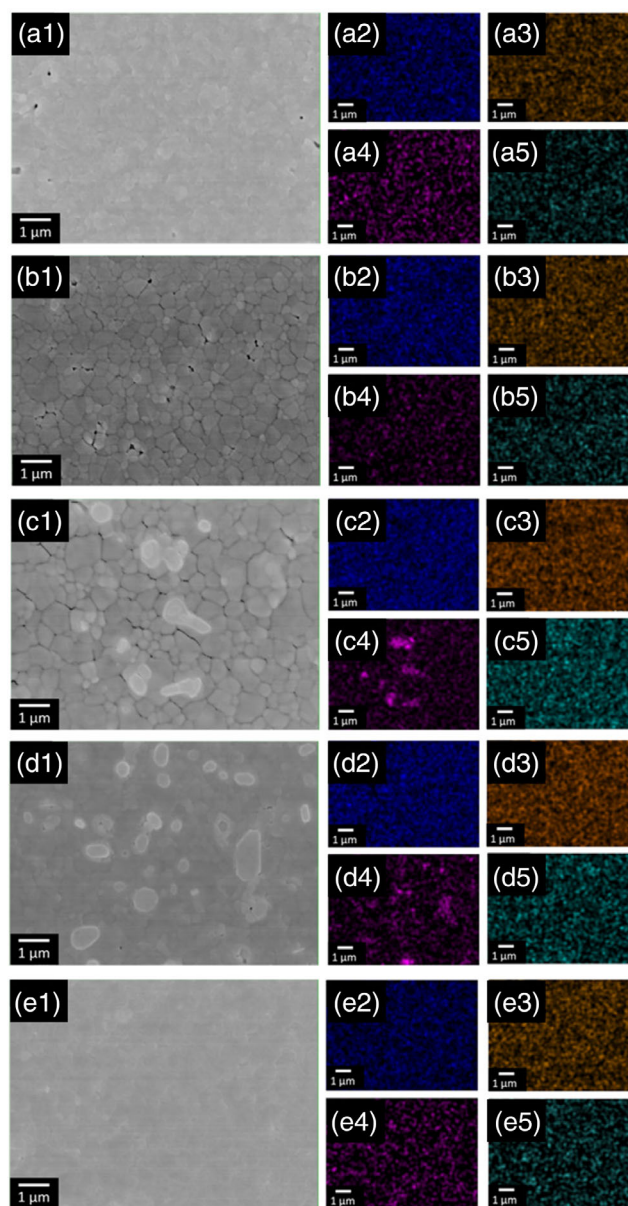


Figure 5. a1–e1) FE-SEM images and EDS mapping of different element, including a2–e2) Pb, a3–e3) I, a4–e4) Cl, and a5–e5) Ba of a) PVK, b) Ba/PVK, c) Ba/PVK-V, d) Ba/PVK-M, and e) Ba/PVK-E active layer, respectively.

the *V*_{oc}, *J*_{sc}, and FF would suddenly drop. This result was consistent with our previous study. Some pinholes would start to appear in the films, leading to poorer film formation and thus resulted in poorer photovoltaic performance.^[21,22,50] Therefore, the lead replacement amount is still limited, the Ba doping amount could only reach 5.0 mol% to obtain the PSCs with desirable performance.

We want to further boost the ratio of Ba²⁺ while achieving considerable device efficiency. Therefore, according to our preliminary results, we tried to modify the 10.0 mol% Ba-doped PSCs (abbreviated as Ba/PVK), which also showed a moderate photovoltaic performance (PCE > 13%), by introducing various

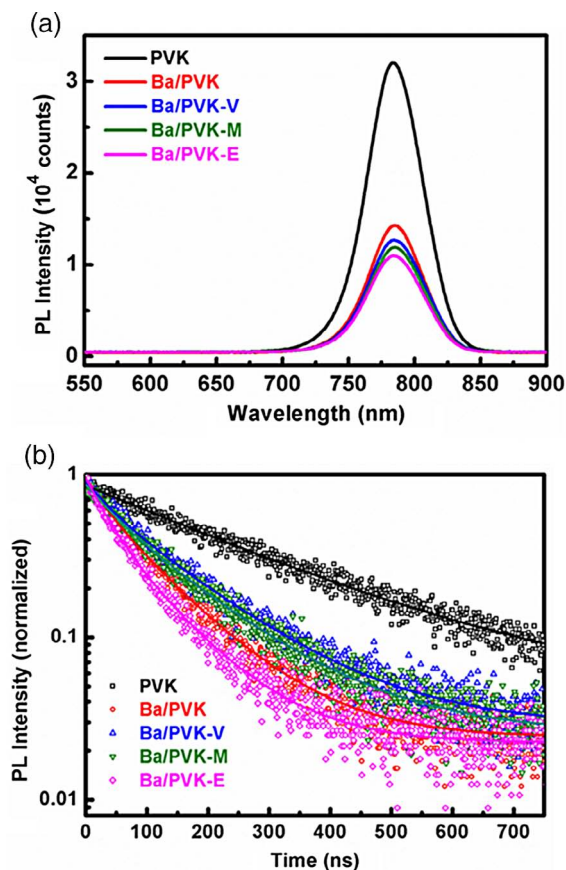


Figure 6. a) Photoluminescence spectra and b) time-resolved photoluminescence spectra of PVK, Ba/PVK, Ba/PVK-V, Ba/PVK-M, and Ba/PVK-E films coating on FTO/meso-Zn:TiO₂.

Table 1. Summary of measured fast and slow decay time and PL average decay for the perovskite films coated on FTO/meso-Zn:TiO₂.

Active layer	Polymer additive	A ₁ [%]	τ_1 [ns]	A ₂ [%]	τ_2 [ns]	τ_{avg} [ns]
PVK	–	50.0	263.7	50.0	263.7	263.7
Ba/PVK	–	24.3	33.7	75.7	109.6	91.2
Ba/PVK-V	P(VDF-TrFE)	22.5	39.5	77.5	146.6	122.5
Ba/PVK-M	PMMA	24.5	47.1	75.5	142.9	119.4
Ba/PVK-E	PEG	43.1	35.8	56.9	99.7	72.2

polymer additives to improve surface morphology. Three kinds of polymers were selected as polymer additives in this study, including P(VDF-TrFE), PMMA, and PEG. When P(VDF-TrFE), PMMA, and PEG were added into the 10.0 mol% Ba/PVK device (which are abbreviated as Ba/PVK-V, Ba/PVK-M, and Ba/PVK-E, separately), it was easily observed that the V_{oc} of all devices were nearly the same (Figure 2a). These results meant that small amounts of additives could not affect the bandgap of the perovskite active layer. However, with Ba doping, the J_{sc} increased but the FF decreased, and the pinholes and defects on the film would lead to current leakage and thus lead to lower FF. With P(VDF-TrFE) and PMMA as polymer additives doping

into the Ba-doped device, the FF would increase significantly. Yet the J_{sc} of PMMA and P(VDF-TrFE)-doped devices significantly decreased. As for PEG-doped device, J_{sc} and FF were both enhanced and had the best device performance.

Figure 2b shows the PCE distribution of PVK, Ba/PVK, Ba/PVK-V, Ba/PVK-M, and Ba/PVK-E devices. P(VDF-TrFE) (MW \approx 450 000 Da, 30 mol% TrFE), PMMA (MW \approx 996 000 Da), and PEG (MW \approx 10 000 Da) were doped into the Ba/PVK device at various concentrations to optimize the best doping concentration (Figure S1, Supporting Information). We found that the optimized concentrations of P(VDF-TrFE) and PMMA were 10^{−3} and 10^{−4} wt%, respectively. From the aforementioned results, the device with PEG doping had the best performance. Consequently, PEG with various molecular weights (MW \approx 1500, \approx 10 000, and \approx 20 000 Da) were examined to test the best parameter for PEG as a polymer additive. From the J – V curves and PCE distributions, PEG with a molecular weight of 10 000 was most useful as a polymer additive, and the optimized concentration of PEG was 10^{−3} wt%.

To investigate the surface morphology of various films, field-emission scanning electron microscope (FE-SEM) images were taken (Figure 3, left column). The corresponding cross-section SEM image of PSC is shown in Figure S2, Supporting Information. Many grains could be seen on the pristine (Figure 3a and Figure S2a, Supporting Information) film. When Ba was doped (Figure 3b and Figure S2b, Supporting Information), several pinholes could be observed in the Ba-doped film due to excessive Ba doping.^[22] From Figure 3c,d and Figure S2c and S2d, Supporting Information, the films with P(VDF-TrFE) and PMMA doping have fewer pinholes, but phase separation occurs in the perovskite films. Some significant aggregation can be seen on the surfaces, which were speculated to be the P(VDF-TrFE) and PMMA precipitates resulted from poor solubility of the polymer in perovskite solutions. The non-conductive precipitations (the brighter parts) became obstacles for electron transport, which also led to poor performance and poor long-term stability of the perovskite device. However, no precipitate existed on the PEG-doped film surface (Figure 3e and Figure S2e, Supporting Information), which was uniform without pinholes, making it a superior candidate as a polymer additive.

In addition, to check whether the big aggregation on the surface belonged to the perovskite phase or not, backscattered electron (BSE) images of the perovskite films were taken (Figure 3, middle column). The P(VDF-TrFE) (Figure 3c) and PMMA (Figure 3d) films show the obvious aggregation with darker color. However, BSE images of the PVK, Ba/PVK, and Ba/PVK-E films (Figure 3a,b,e), which were the same phases as those of the P(VDF-TrFE) and PMMA films, exhibited no precipitation. Thus, the PEG exhibited good solubility in perovskite film.

Atomic force microscope (AFM) images taken in tapping mode were used to determine the roughness of the perovskite films (Figure 3, right column). When Ba was doped into the perovskite film, the root-mean-square (RMS) roughness decreased from 56.7 nm (pristine) to 41.0 nm. From the AFM images, the polymer additives were able to modify the perovskite morphology, resulting in lower RMS roughness. The RMS roughness of the Ba/PVK-V, Ba/PVK-M, and Ba/PVK-E films were 35.7, 31.1, and 28.9 nm, respectively. The RMS roughness

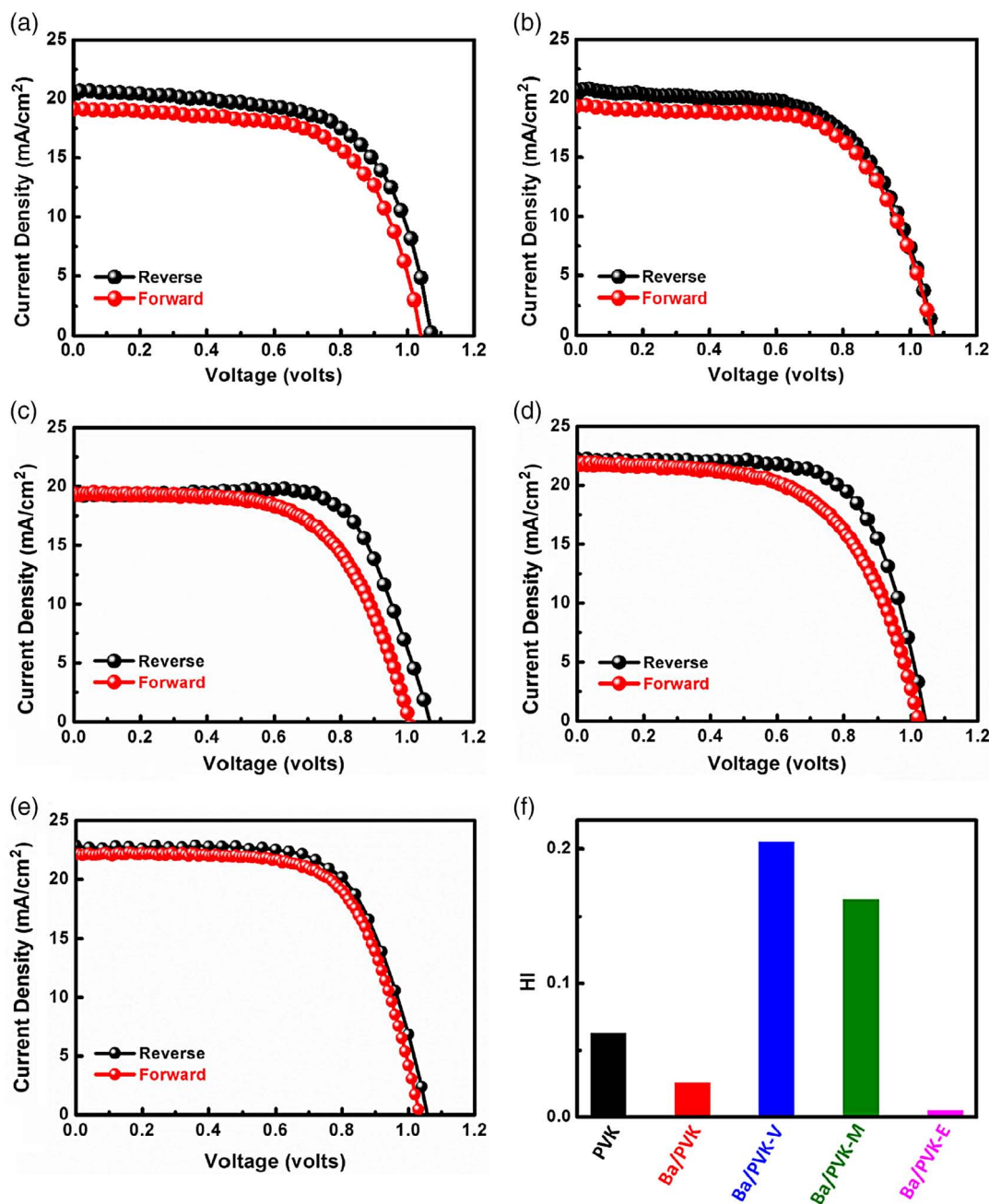


Figure 7. *J*–*V* curves of a) PVK, b) Ba/PVK, c) Ba/PVK-V, d) Ba/PVK-M, and e) Ba/PVK-E devices with reverse and forward scans. f) HI comparison of PVK, Ba/PVK, Ba/PVK-V, Ba/PVK-M, and Ba/PVK-E of PSCs devices.

of Ba/PVK-E film was reduced the most from 41.0 to 28.9 nm, which indicated that PEG had effectively improved the surface morphology.

Figure 4 shows the X-ray diffractometer (XRD) analysis, which was measured to recognize the phases in perovskite materials and crystallite sizes. All samples had the perovskite peaks at 14.5° and 29.0°, which represented the planes of (110) and (220), respectively. For the PVK film, the peak of δ -FAPbI₃ phase (at 13.0°) appeared. However, when Ba was partially doped, the peak of the instable δ -FAPbI₃ phase disappeared on the XRD

pattern, indicating that the introduction of Ba-assisted PbI₂ to transfer into the perovskite phase completely. For the films with P(VDF-TrFE), PMMA, and PEG doping, the peaks of δ -FAPbI₃ phase did not appear on the XRD patterns as well. However, the intermediate phase of Ba/PVK-V and Ba/PVK-M films appeared at 16.5°. The incomplete phase transformation maybe because the precipitates of PMMA and P(VDF-TrFE) inhibit the crystallization of perovskite. As for Ba/PVK-E film, there was no impurity peak on the XRD pattern, and the perovskite peak intensity signal at 14.5° significantly increased, leading to a higher crystallinity.

The crystallite sizes of various perovskite films (Figure 4b) were calculated by Scherrer equation.^[51] The crystallite size for the pristine film was 57.2 nm, but the crystallite size for the Ba-doped film decreased to 44.5 nm. With the modification of polymer additives, the crystallite sizes increased to 61.6, 61.6, and 57.2 nm for the Ba/PVK-V, Ba/PVK-M, and Ba/PVK-E films, respectively. Although the crystallite size of Ba/PVK-E film did not increase the most, the increased size was able to form a uniform film with fewer boundaries and pinholes on the surface and led to a high photovoltaic performance.

We also investigated the absorption in the visible light region (Figure S3a, Supporting Information). From the UV-vis absorption spectra, the Ba-doped film showed a redshift. For the polymer-doped films, the absorbance of the films was increased in the visible-light region, due to the better morphology without pinholes (Figure 3c–e). The Tauc plot was transferred from the absorption spectra to calculate the bandgap of each sample (Figure S3b, Supporting Information). The pristine film has a bandgap of 1.48 eV; however, with the Ba doping, the bandgap decreased to 1.46 eV. According to previous studies, when alkaline earth metal is doped, it leads to an energy-level change in perovskite material and a reduction in the bandgap.^[21,22] For the Ba-doped film with polymer additives, the bandgap slightly decreased to 1.45 eV for all three kinds of polymers. The bandgap decrease in the Ba-doped film was related to the presence of the dopants slightly modifying the interaction with the ions in the network.

The energy-dispersive X-ray spectroscopy (EDS) analysis of the various perovskite active layers was made to investigate the chemical composition of the precipitates in the perovskite film. From EDS mapping images and XRD patterns, we found that the precipitates in Ba/PVK-V and Ba/PVK-M active layers would only accumulate in the element spectra of chloride (Figure 5). As a result, we speculated that the precipitates were chloride derivatives. As for Ba-PEG film, no accumulation was seen in the EDS mapping images of chloride.

Figure 6 shows photoluminescence (PL) spectra and time-resolved PL (TRPL) spectra of various fluorine-doped tin oxide (FTO)/meso-Zn:TiO₂/perovskite to investigate the charge carrier dynamics. The PL intensity significantly decreased with Ba doping. When polymer additives were added into the Ba/PVK active layer, the PL intensity further decreased to a lower level, especially PEG-doped film. For the TRPL spectra, we used the biexponential decay function to fit the TRPL spectra.^[52] The TRPL spectra fitting results are shown in Table 1. Ba/PVK film shows a lifetime of 91.2 ns. However, the decay lifetimes of Ba/PVK-V (122.5 ns) and Ba/PVK-M (119.4 ns) films were not faster compared with that of the Ba/PVK film without polymer additives as expected. To explain this phenomenon, two situations can be considered: for situation 1, when the polymer additives are doped, they are able to modify the surface morphology to improve the electron transport and have shorter decay lifetime.^[53] For situation 2, impurities are formed to hinder the electron generation, which may result in lower PL intensity and longer decay lifetime. For Ba/PVK-E film, it belongs to situation 1, where doping has successfully improved the morphology, resulting in the lowest PL intensity and the shortest PL average lifetime (τ_{avg}) of 72.2 ns. As for the cases of Ba/PVK-V and Ba/PVK-M films, they belong to situation 2. The P(VDF-TrFE) and PMMA-doped films had lower PL

intensity comparing with the Ba/PVK film; however, they had longer τ_{avg} of 122.5 and 119.4 ns. To further compare these two situations, we measured the PL spectra of silicon wafer/perovskite and the PL spectra are shown in Figure S4, Supporting Information. The Ba/PVK-E film demonstrates the highest PL intensity, which means that the addition of PEG to the perovskite film can improve the carrier generation. In contrast, Ba/PVK-V and Ba/PVK-M films still show lower PL intensity, which means that impurities hinder electron generation. Thus, it can be concluded that from PL and TRPL spectra, PEG is the most suitable polymer additive that can successfully enhance the surface morphology without pinholes and will not become an obstacle for charge transportation.

The *J*–*V* curves of the PVK, Ba/PVK, Ba/PVK-V, Ba/PVK-M, and Ba/PVK-E for both forward and reverse scans are shown in Figure 7 and the photovoltaic performances of various perovskite devices are shown in Table 2. With Ba doping, the HI decreased from 0.063 (Figure 7a) to 0.026 (Figure 7b), indicating little to no hysteresis effect that could be ignored. However, with P(VDF-TrFE) (Figure 7c) and PMMA (Figure 7d) doping, the HI severely increased to 0.205 and 0.162, respectively. The higher HI of Ba/PVK-V and Ba/PVK-M devices were due to precipitates acting as obstacles, blocking the route for efficient charge transportation. Moreover, it could be observed that the HI increased with higher hydrophobicity of the polymer additives. As a result, the HI of Ba/PVK-V device was higher than that of the Ba/PVK-M device. The *J*–*V* curves of the Ba/PVK-E champion device in reverse and forward scans are shown in Figure 7e. The PCE of the Ba/PVK-E champion device was enhanced from 13.7% (without polymer additive) to 16.1% with a higher FF of 66.8%. Therefore, it can be concluded that with a hydrophilic polymer as a polymer additive, such as PEG, the hysteresis effect can be effectively reduced to an ignorable extent.

To investigate the morphology change in the ambient atmosphere, the perovskite films and devices were stored in a moisture-proof box (25 °C and 20–30% RH). We observed the perovskite surface using optical microscopy at various time (1, 5, 10, 20, and 30 days; Figure 8a–e). It could be observed that the PVK film morphology did not change remarkably, except for several pinholes appearing on the surface (Figure 8a1–a5).

Table 2. Photovoltaic performance of PSCs with various perovskite active layer.

Sample name	Scan direction	J_{sc} [mA cm ⁻²]	V_{oc} [V]	FF [%]	PCE [%]	HI
PVK	Reverse	20.7	1.07	63.2	14.0	0.063
	Forward	19.2	1.04	63.2	12.6	
Ba/PVK	Reverse	20.7	1.07	61.9	13.7	0.026
	Forward	19.4	1.07	63.6	13.1	
Ba/PVK-V	Reverse	19.3	1.07	70.6	14.5	0.205
	Forward	19.4	1.01	62.0	12.1	
Ba/PVK-M	Reverse	22.2	1.04	68.0	15.8	0.162
	Forward	21.9	1.02	59.3	13.3	
Ba/PVK-E	Reverse	22.9	1.06	66.8	16.1	0.005
	Forward	22.1	1.03	66.9	15.3	

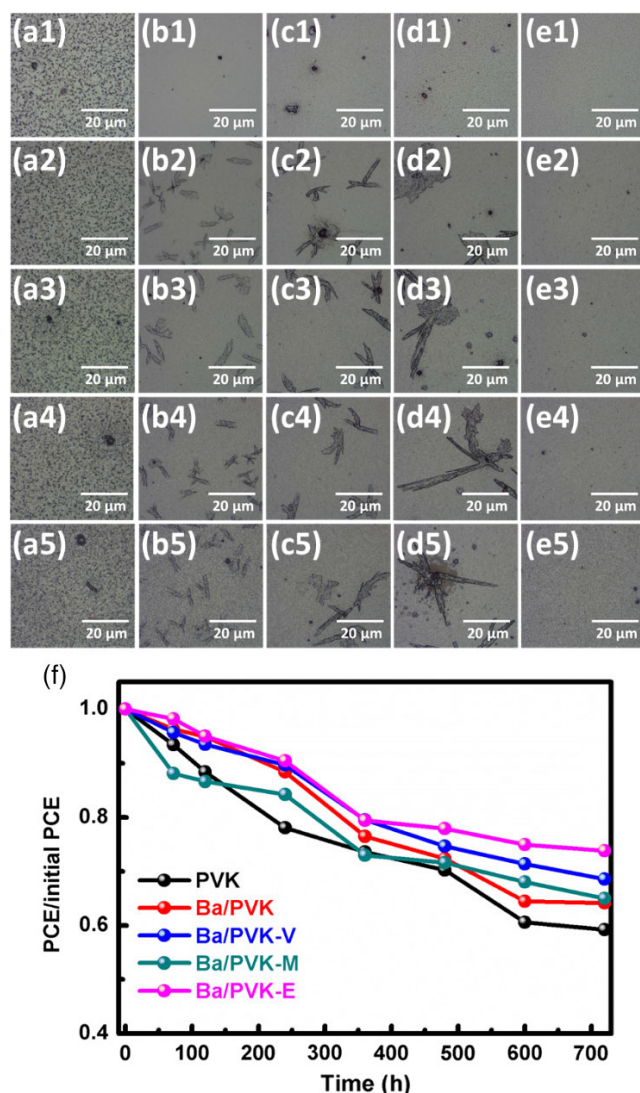


Figure 8. Perovskite films of a) PVK, b) Ba/PVK, c) Ba/PVK-V, d) Ba/PVK-M, and e) Ba/PVK-E observed by OM after 1, 5, 10, 20, and 30 days. The samples were stored in an ambient atmosphere. f) Long-term stability of PVK, Ba/PVK, Ba/PVK-V, Ba/PVK-M, and Ba/PVK-E devices after 720 h (30 days). The devices were stored in the ambient air with RH 20–30% (25 °C).

Moreover, the surface of PVK film was rougher than the Ba/PVK film. For the Ba/PVK film, the film surface (Figure 8b1) was much smoother than the pristine film (Figure 8a1) on day 1. It was interesting that starting on day 5, there would be some “dragonfly-like” objects appearing on the surface, and these objects likely expanded from small pinholes (Figure 8b2). The same situations could be observed on the P(VDF-TrFE) and PMMA-doped films (Figure 8c,d). However, due to the improved morphology with polymer additives, the quantities of such objects were reduced, resulting in better stability. On the Ba/PVK-M film, the same objects were fewer but slightly more prominent. As for the Ba/PVK-V film, bigger but less of these objects were present. If the number of such objects increased, it was speculated that these objects expanded from pinholes, and were the result of poor stability. For the PEG-doped film, it could be observed that the

films were nearly unchanged from day 1, except for several small pinholes (Figure 8e1–e5). This result indicated that the PEG-doped film possessed better morphology and excellent stability. Long-term stability is another critical factor to consider while measuring PSCs performance (Figure 8f). The devices were kept in ambient air with 20–30% RH and 25 °C. From the long-term stability figure, all devices had remained excellent stability after 720 h, especially for the Ba/PVK-E device. The Ba/PVK-E device had high stability which maintained 74% of its initial PCE after 720 h, which was corresponding to the morphology change images from OM as well (Figure 8e1–e5). In addition, we also measured the 5 days stability with standard deviation of nine devices for each perovskite active layer (Figure S5, Supporting Information). After 5 days, all devices maintain >90% of its initial PCE. Especially, the Ba/PVK-E devices demonstrate outstanding average PCE, which shows >95% of its initial PCE after 5 days (Figure S5e, Supporting Information).

3. Conclusion

To reduce the toxicity of Pb-based perovskite device, it is desired to develop a compact perovskite thin film with a higher doping ratio of Ba. We found that although the 10.0 mol% Ba-doped device had high V_{oc} and J_{sc} , it had a lower FF, which was mainly due to the defects on the perovskite layer. Fortunately, by introducing various polymer additives to the 10.0 mol% Ba-doped mixed-cation PSCs, the morphology significantly improved, leading to enhanced FF of the device. P(VDF-TrFE), PMMA, and PEG were selected as polymer additives to be doped into the 10.0 mol% Ba-doped mixed-cation perovskite due to their outstanding properties. When P(VDF-TrFE) and PMMA were doped, some precipitates appeared on the surface, which became obstacles for charge transportation. With PEG, a water-soluble polymer, as polymer additive, it merged with the 10.0 mol% Ba-doped perovskite perfectly. It showed better morphology without pinholes or precipitates on the surface. Finally, we have successfully modified the 10.0 mol% Ba-doped mixed-cation PSCs with PEG. The PCE of Ba/PVK-E champion device was enhanced from 13.7% (without polymer additive) to 16.1% with long-term stability. With significant enhancement on the lead-reduced mixed-cation PSCs, it is much eco-friendlier to the environment and possesses the enormous potential of PSCs commercialization in the future.

4. Experimental Section

Materials: Acetonitrile (ACN, 99.5%), ethyl cellulose (EC, ethoxyl content 48%, 22 cps), and poly(ethylene glycol) (PEG, MW 1500) were purchased from ACROS. Lead iodide (PbI₂, 99.9985%) and PEG (MW 10 000 and 20 000) were purchased from Alfa Aesar. α -terpineol (C₁₀H₁₈O, 90%) was purchased from Merck. Dimethyl sulfoxide (DMSO, 99.9%) and zinc nitrate hexahydrate (Zn(NO₃)₂·6H₂O, >97%) were purchased from ECHO. The 2,2',7,7'-tetrakis[N,N-di(4-methoxy-phenyl)amino]-9,9'-spirobifluorene (spiro-OMeTAD) was purchased from Frontier Materials. P(VDF-TrFE) (Piezotech FC 30) was purchased from Piezotech. Barium iodide (BaI₂, 99.995%), γ -butyrolactone (GBL, ≥99%), lead chloride (PbCl₂, 99.999%), lithium-bis-(trifluoromethanesulfonyl)imide (Li-TFSI, 99.95%), 4-*tert*-butylpyridine (tBP, 96%), titanium diisopropoxide bis(acetylacetonate) ((CH₃)₂CHO)Ti(C₅H₇O₂)₂, 75 wt% in ethanol),

titanium isopropoxide ($\text{Ti}(\text{OCH}(\text{CH}_3)_2)_4$, >97%, Sigma-Aldrich), and poly(methyl methacrylate) (PMMA, MW 120 000, 350 000, and 996 000) were purchased from Sigma-Aldrich. The 2-propanol ($(\text{CH}_3)_2\text{CHOH}$, IPA, >99.8%, STAREK), FA iodide (FAI, >98%), and methylammonium iodide (MAI, >98%) were purchased from STAREK. Chlorobenzene (CB, 99.9%) was purchased from Tedia. All the materials and solvents used in this study were used as received without any further purification.

Sample Preparation: The synthesis of mesoporous zinc-doped TiO_2 (meso-Zn: TiO_2) paste was based on our previous work.^[54] Briefly, a 12.5 g of titanium isopropoxide and 5.0 mL of 2-propanol were mixed together. Zinc nitrate hexahydrate was added in a 90.0 mL of 3.5 M acetic acid solution. Then, the zinc precursor solution was dropped into the titanium precursor solution in continuous stirring in an ice bath for 12 h. The transparent solution was heated at 80 °C for 8 h. The white translucent solution was treated in an autoclave at 170 °C for 6 h, and it was centrifuged to obtain Zn: TiO_2 nanoparticles (NPs). A 23.0 wt% of Zn: TiO_2 NPs was mixed with α -terpineol and EC, then the excess solvent was removed by rotary evaporation. For polymer-DMSO solution preparation, a 2.0 wt% of polymer additive was dissolved in DMSO in a water bath at 80 °C to prepare polymer-DMSO solution. For polymer-DMSO preparation, we have individually dissolved each of PMMA, P(VDF-TrFE), and PEG in DMSO separately to form PMMA-DMSO, P(VDF-TrFE)-DMSO, and PEG-DMSO solutions. The polymer-DMSO solutions were covered with aluminum foil to avoid irradiation from light. For perovskite precursor solutions preparation, a 1.7 M mixed-cation perovskite precursor solution was prepared to dissolve by MAI/FAI (molar ratio = 0.4:0.6) and $\text{PbI}_2/\text{PbCl}_2$ (molar ratio = 0.9:0.1) in a mixture of GBL/DMSO (1.0/1.0 v/v). The mixed-cation lead-reduced perovskite precursor solution was to have PbI_2 partially replaced by BaI_2 at the various doping concentration (5.0, 10.0, and 15.0 mol%). The solvent of mixed-cation lead-reduced perovskite precursor solution with polymer additives changed DMSO into polymer-DMSO solutions. The perovskite precursor solutions were then stirred at 45 °C overnight. For hole transport layer precursor solution preparation, 80.0 mg spiro-OMeTAD, 28.5 mL tBP, and 17.5 μL Li-TFSI solution (104 mg of Li-TFSI dissolved in 200 μL of ACN) prepared previously were dissolved in 1.0 mL of CB under continuous stirring.

PSCs Fabrication: The FTO glass (7 Ω , FrontMaterials Co. Ltd.) was cleaned by detergent, acetone, and isopropanol sequentially. After cleaning, the FTO was blow-dried by an air gun and treated with UV-ozone for 20 min. The dense TiO_2 layer was completed by spray-coating the 0.05 M titanium diisopropoxide bis(acetylacetonate) solution on the FTO glass at 450 °C twice. The diluted 5.0 mol% meso-Zn: TiO_2 paste (1/6 v/v in α -terpineol) was screen-printed on the dense TiO_2 layer, and transferred to the laboratory oven at 125 °C for 10 min. Finally, the substrate was calcined at 500 °C for 30 min right away to finish the electron transport layer. The prepared perovskite precursor solution was spin-coated on the meso-Zn: TiO_2 layer at 1000 rpm for 10 s and 5000 rpm for 20 s. At the second step of spin-coating, 300 μL of CB was dropped onto the perovskite absorbing layer as antisolvent at 13 s and the substrates were then annealed at 100 °C for 10 min right away. The spiro-OMeTAD precursor solution was spin-coated onto the perovskite absorbing layer at 2500 rpm for 30 s. Subsequently, 120 nm of the silver electrode was thermally evaporated onto the spiro-OMeTAD layer with a 0.09 cm^2 shadow mask.

Characterization and Measurement of Materials and Devices: The J - V curves of various devices were measured by a digital source meter (2400, Keithley) under simulated solar illumination at 100 mW cm^{-2} , AM 1.5G standard. The light source was calibrated with a Si-reference cell (BS-520BK, Bunkoiki) with KG-5 filter. The reverse scan and forward scan J - V curves were measured from 1.2 to -0.1 V and -0.1 to 1.2 V, respectively. The step voltage was set at 10 mV, and the delay time was set at 500 ms. The surface morphology and microstructure of the perovskite films were observed by FE-SEM (SU8010, Hitachi) with an accelerating voltage of 10 kV. The surface roughness of the perovskite films was analyzed by AFM (Dimension-3100 Multimode, Digital Instruments) in tapping mode. The absorption spectra were obtained by a UV-vis spectrometer (V-730, Jasco). The steady-state PL spectra were obtained by a continuous-wave diode laser beam ($\lambda_{\text{exc}} = 440 \text{ nm}$, PDLH-

440-25, Dongwoo Optron Co. Ltd.) hitting on the samples. The photomultiplier tube detector system and standard photon-counting electronics with a monochromator were used to obtain the emission spectra. TRPL spectra were measured by a time-correlated single-photon counting spectrometer (WELLS-001 FX, Dongwoo Optron Co. Ltd.). A pulse laser (440 nm) with an average power of 1 mW was operating under 312.5 MHz with a 2 μs duration using for excitation. The crystal structure and phase identification were determined by XRD (D2 Phaser, Bruker). The EDS (XFlash 5030, Bruker) analysis was operated to investigate the elements containing in various perovskite films.

Supporting Information

Supporting Information is available from the Wiley Online Library or from the author.

Acknowledgements

M.-C.W. and Y.-Y.L. contributed equally to this work. The authors appreciate Dr. Ming-Tao Lee group and Dr. Jyh-Fu Lee group (BL-13A1 and BL-17C) at National Synchrotron Radiation Research Center for useful discussion and suggestions. The financial support from Ministry of Science and Technology of Taiwan (project nos. 106-2221-E-182-057-MY3, 108-3116-F-002-002-CC2, and 108-2119-M-002-005), Industrial Technology Research Institute, Chang Gung University (grant no. QZRPD181), and Chang Gung Memorial Hospital, Linkou (grant nos. CMRPD2H0162 and BMRPC74) is highly appreciated.

Conflict of Interest

The authors declare no conflict of interest.

Keywords

perovskite solar cells, polymer additives, power conversion efficiency, stability

Received: February 17, 2020

Revised: March 9, 2020

Published online:

- [1] NREL: Best-Research-Cell-Efficiencies, <https://www.nrel.gov/pv/assets/pdfs/best-research-cell-efficiencies.20200311.pdf> (accessed: March 2020).
- [2] D. P. McMeekin, G. Sadoughi, W. Rehman, G. E. Eperon, M. Saliba, M. T. Höranter, A. Haghighirad, N. Sakai, L. Korte, B. Rech, M. B. Johnston, L. M. Herz, H. J. Snaith, *Science* **2016**, 351, 151.
- [3] H. J. Snaith, *J. Phys. Chem. Lett.* **2013**, 4, 3623.
- [4] X. Li, D. Bi, C. Yi, J.-D. Décoppet, J. Luo, S. M. Zakeeruddin, A. Hagfeldt, M. Grätzel, *Science* **2016**, 353, 58.
- [5] J. Feng, X. Zhu, Z. Yang, X. Zhang, J. Niu, Z. Wang, S. Zuo, S. Priya, S. Liu, D. Yang, *Adv. Mater.* **2018**, 30, 1801418.
- [6] C. Quarti, E. Mosconi, J. M. Ball, V. D'Innocenzo, C. Tao, S. Pathak, H. J. Snaith, A. Petrozza, F. De Angelis, *Energy Environ. Sci.* **2016**, 9, 155.
- [7] S.-H. Turren-Cruz, M. Saliba, M. T. Mayer, H. Juárez-Santisteban, X. Mathew, L. Nienhaus, W. Tress, M. P. Erodici, M.-J. Sher, M. G. Bawendi, M. Grätzel, A. Abate, A. Hagfeldt, J.-P. Correa-Baena, *Energy Environ. Sci.* **2018**, 11, 78.
- [8] D.-H. Kang, N.-G. Park, *Adv. Mater.* **2019**, 31, 1805214.

- [9] B.-W. Park, S. I. Seok, *Adv. Mater.* **2019**, *31*, 1805337.
- [10] P. Billen, E. Leccisi, S. Dastidar, S. Li, L. Lobaton, S. Spataro, A. T. Fafarman, V. M. Fthenakis, J. B. Baxter, *Energy* **2019**, *166*, 1089.
- [11] J. Xu, O. Voznyy, R. Comin, X. Gong, G. Walters, M. Liu, P. Kanjanaboos, X. Lan, E. H. Sargent, *Adv. Mater.* **2016**, *28*, 2807.
- [12] E. L. Unger, E. T. Hoke, C. D. Bailie, W. H. Nguyen, A. R. Bowring, T. Heumüller, M. G. Christoforo, M. D. McGehee, *Energy Environ. Sci.* **2014**, *7*, 3690.
- [13] H.-S. Kim, N.-G. Park, *J. Phys. Chem. Lett.* **2014**, *5*, 2927.
- [14] W. Li, J. Liu, F.-Q. Bai, H.-X. Zhang, O. V. Prezhdo, *ACS Energy Lett.* **2017**, *2*, 1270.
- [15] G. Niu, X. Guo, L. Wang, *J. Mater. Chem. A* **2015**, *3*, 8970.
- [16] M.-C. Wu, S.-H. Chan, T.-F. Lin, C.-F. Lu, W.-F. Su, *J. Taiwan Inst. Chem. Eng.* **2017**, *78*, 552.
- [17] M. Chen, M.-G. Ju, H. F. Garces, A. D. Carl, L. K. Ono, Z. Hawash, Y. Zhang, T. Shen, Y. Qi, R. L. Grimm, D. Pacifici, X. C. Zeng, Y. Zhou, N. P. Padture, *Nat. Commun.* **2019**, *10*, 16.
- [18] F. Yang, M. A. Kamarudin, G. Kapil, D. Hirotani, P. Zhang, C. H. Ng, T. Ma, S. Hayase, *ACS Appl. Mater. Interfaces* **2018**, *10*, 24543.
- [19] C. F. J. Lau, X. Deng, J. Zheng, J. Kim, Z. Zhang, M. Zhang, J. Bing, B. Wilkinson, L. Hu, R. Patterson, S. Huang, A. Ho-Baillie, *J. Mater. Chem. A* **2018**, *6*, 5580.
- [20] T. J. Jacobsson, M. Pazoki, A. Hagfeldt, T. Edvinsson, *J. Phys. Chem. C* **2015**, *119*, 25673.
- [21] M.-C. Wu, W.-C. Chen, S.-H. Chan, W.-F. Su, *Appl. Surf. Sci.* **2018**, *429*, 9.
- [22] S.-H. Chan, M.-C. Wu, K.-M. Lee, W.-C. Chen, T.-H. Lin, W.-F. Su, *J. Mater. Chem. A* **2017**, *5*, 18044.
- [23] M. Pazoki, T. Edvinsson, *Sustainable Energy Fuels* **2018**, *2*, 1430.
- [24] K. Wang, W. S. Subhani, Y. Wang, X. Zuo, H. Wang, L. Duan, S. Liu, *Adv. Mater.* **2019**, *31*, 1902037.
- [25] S. S. Mali, J. V. Patil, C. K. Hong, *Nano Lett.* **2019**, *19*, 6213.
- [26] S. Kajal, G.-H. Kim, C. W. Myung, Y. S. Shin, J. Kim, J. Jeong, A. Jana, J. Y. Kim, K. S. Kim, *J. Mater. Chem. A* **2019**, *7*, 21740.
- [27] W. S. Subhani, K. Wang, M. Du, S. F. Liu, *Nano Energy* **2019**, *61*, 165.
- [28] J. Qin, Z. Zhang, W. Shi, Y. Liu, H. Gao, Y. Mao, *ACS Appl. Mater. Interfaces* **2018**, *10*, 36067.
- [29] C.-Y. Chang, C.-Y. Chu, Y.-C. Huang, C.-W. Huang, S.-Y. Chang, C.-A. Chen, C.-Y. Chao, W.-F. Su, *ACS Appl. Mater. Interfaces* **2015**, *7*, 4955.
- [30] J. Jiang, Q. Wang, Z. Jin, X. Zhang, J. Lei, H. Bin, Z.-G. Zhang, Y. Li, S. Liu, *Adv. Energy Mater.* **2018**, *8*, 1701757.
- [31] D. Wang, L. Zhang, K. Deng, W. Zhang, J. Song, J. Wu, Z. Lan, *Energy Technol.* **2018**, *6*, 2380.
- [32] T.-H. Han, J.-W. Lee, C. Choi, S. Tan, C. Lee, Y. Zhao, Z. Dai, N. De Marco, S.-J. Lee, S.-H. Bae, Y. Yuan, H. M. Lee, Y. Huang, Y. Yang, *Nat. Commun.* **2019**, *10*, 520.
- [33] S. Valero, T. Soria, N. Marinova, J. L. Delgado, *Polym. Chem.* **2019**, *10*, 5726.
- [34] Y. Zhao, J. Wei, H. Li, Y. Yan, W. Zhou, D. Yu, Q. Zhao, *Nat. Commun.* **2016**, *7*, 10228.
- [35] Y. Zhao, Q. Li, W. Zhou, Y. Hou, Y. Zhao, R. Fu, D. Yu, X. Liu, Q. Zhao, *Sol. RRL* **2019**, *3*, 1800296.
- [36] E. Jia, D. Wei, P. Cui, J. Ji, H. Huang, H. Jiang, S. Dou, M. Li, C. Zhou, W. Wang, *Adv. Sci.* **2019**, *6*, 1900252.
- [37] C.-C. Zhang, Z.-K. Wang, S. Yuan, R. Wang, M. Li, M. F. Jimoh, L.-S. Liao, Y. Yang, *Adv. Mater.* **2019**, *31*, 1902222.
- [38] X. Zhang, Y. Zhou, Y. Li, J. Sun, X. Lu, X. Gao, J. Gao, L. Shui, S. Wu, J.-M. Liu, *J. Mater. Chem. C* **2019**, *7*, 3852.
- [39] C. Wu, K. Wang, Y. Yan, D. Yang, Y. Jiang, B. Chi, J. Liu, A. R. Esker, J. Rowe, A. J. Morris, M. Sanghadasa, S. Priya, *Adv. Funct. Mater.* **2019**, *29*, 1804419.
- [40] Y. Ko, Y. Kim, C. Lee, Y. Kim, Y. Jun, *Synth. Met.* **2019**, *249*, 47.
- [41] Q. Fu, S. Xiao, X. Tang, Y. Chen, T. Hu, *ACS Appl. Mater. Interfaces* **2019**, *11*, 24782.
- [42] K. Sakthi Velu, J. Anandha Raj, P. Sathappan, B. Suganya Bharathi, S. Mohan Doss, S. Selvam, P. Manisankar, T. Stalin, *Mater. Lett.* **2019**, *240*, 132.
- [43] R. Fu, W. Zhou, Q. Li, Y. Zhao, D. Yu, Q. Zhao, *ChemNanoMat* **2019**, *5*, 253.
- [44] L. Aoudjit, P. M. Martins, F. Madjene, D. Y. Petrovykh, S. Lanceros-Mendez, *J. Hazard. Mater.* **2018**, *344*, 408.
- [45] U. Ali, K. J. B. A. Karim, N. A. Buang, *Polym. Rev.* **2015**, *55*, 678.
- [46] S.-L. Yeh, C.-Y. Zhu, S.-W. Kuo, *Polymers* **2015**, *7*, 1379.
- [47] H. He, S. Chen, J. Bai, H. Zheng, B. Wu, M. Ma, Y. Shi, X. Wang, *RSC Adv.* **2016**, *6*, 34685.
- [48] C. Zhang, X. Liu, H. Liu, Y. Wang, Z. Guo, C. Liu, *Polym. Test* **2019**, *75*, 367.
- [49] Q. Cheng, C. Jiang, J. Zhang, Z. Yang, Z. Zhu, H. Jiang, *Tribol. Int.* **2016**, *101*, 110.
- [50] M.-C. Wu, T.-H. Lin, S.-H. Chan, Y.-H. Liao, Y.-H. Chang, *ACS Appl. Energy Mater.* **2018**, *1*, 4849.
- [51] A. W. Burton, K. Ong, T. Rea, I. Y. Chan, *Microporous Mesoporous Mat.* **2009**, *117*, 75.
- [52] Y. Yang, H. Peng, C. Liu, Z. Arain, Y. Ding, S. Ma, X. Liu, T. Hayat, A. Alsaedi, S. Dai, *J. Mater. Chem. A* **2019**, *7*, 6450.
- [53] A. Liu, K. Liu, H. Zhou, H. Li, X. Qiu, Y. Yang, M. Liu, *Sci. Bull.* **2018**, *63*, 1591.
- [54] M.-C. Wu, S.-H. Chan, K.-M. Lee, S.-H. Chen, M.-H. Jao, Y.-F. Chen, W.-F. Su, *J. Mater. Chem. A* **2018**, *6*, 16920.